The Astrophysical Journal, 760:36 (9pp), 2012 November 20 doi:10.1088/0004-637X/760/1/36

PROBING THE ROLE OF CARBON IN ULTRAVIOLET EXTINCTION ALONG GALACTIC SIGHT LINES

V. S. Parvathi[1,4], U. J. Sofia[2], J. Murthy[3], and B. R. S. Babu[1,5]
[1] Department of Physics, University of Calicut, Kerala 673635, India; veena.makesh@gmail.com, brsbabu@gmail.com
[2] Department of Physics, American University, 4400 Massachusetts Avenue, NW, Washington, DC 20016, USA; sofia@american.edu
[3] Indian Institute of Astrophysics, II Block, Koramangala, Bangalore 560034, India; jmurthy@yahoo.com
Received 2011 December 19; accepted 2012 September 24; published 2012 October 31

ABSTRACT

We report previously undetermined interstellar gas and dust-phase carbon abundances along 15 Galactic sight lines based on archival data of the strong 1334.5323 Å transition observed with the Space Telescope Imaging Spectrograph. These are combined with previously reported carbon measurements along six sight lines to produce a complete sample of interstellar C II measurements determined with the 1334 Å transition. Our data set includes a variety of Galactic disk environments characterized by different extinctions and samples paths ranging over three orders of magnitude in average density of hydrogen ($\langle n(\mathrm{H})\rangle$). Our data support the idea that dust, specifically carbon-based grains, are processed in the neutral interstellar medium. We, however, do not find that the abundance of carbon in dust or the grain-size distribution is related to the strength of the 2175 Å bump. This is surprising, given that many current models have polycyclic aromatic hydrocarbons as the bump-producing dust.

Key words: dust, extinction – ISM: abundances – ISM: clouds – ultraviolet: ISM

Online-only material: color figures

1. INTRODUCTION

Carbon is an important element in the interstellar medium (ISM) that exists in several phases in the ISM: dust, gaseous atoms/ions, and gaseous molecules. The phase distribution of carbon is a fundamental characteristic of interstellar clouds that governs their physics. In its gaseous form, carbon plays a crucial role in interstellar molecular chemistry (Snow & Bierbaum 2008) and interstellar cloud cooling is dominated by the rotational and fine structure lines of CO and C II (Bakes & Tielens 1994). Carbon in dust is considered as one of the main candidates responsible for the interstellar ultraviolet (UV) extinction (Draine 1989; Duley & Williams 1981; Joblin et al. 1992). The abundance determination of carbon in the gas and dust phases of the ISM is fundamental to the understanding of physics occurring in the ISM and to the identification of the role of carbon in interstellar extinction. As the direct measurement of carbon abundance in dust is difficult to carry out in the diffuse ISM, gaseous absorption lines of carbon are used as secondary estimators.

The dominant ionization state of carbon in diffuse neutral interstellar clouds (clouds containing H I and H_2) is C II (ionization energy = 11.26 eV). C II is formed when C I is photoionized by the far-UV (FUV) fluxes generated by O and B stars. All of the transitions of C II that are useful for absorption-line studies are in the UV but are either very strong or very weak (Table 1). 13 of the 20 neutral cloud interstellar carbon abundances in the literature are determined from the weak 2325 Å transition of C II (Cardelli et al. 1993, 1996; Hobbs et al. 1982; Sofia et al. 1997, 1998, 2004); one determination is from the 158 μm emission (Dwek et al. 1997) of C II. The remaining six are from Sofia et al. (2011), described further below. Absorption lines from the weak transition have been most commonly used for abundance derivations, but these measurements are few in number because of the need for high spectral resolution and high signal-to-noise observations. As a result, in spite of its importance in ISM studies, the abundance of carbon in the gas and dust phases of the ISM is not well determined.

It is difficult to derive abundances from the strong transitions because of the complex structure and large widths of the absorption lines. It is only recently that Sofia et al. (2011) developed a method to accurately determine interstellar C II and C II* column densities by fitting the strong-line transitions of C II (Table 1) toward the six translucent sight lines. They have compared their results with weak-line abundances along the same lines of sight determined by Sofia et al. (2004) and found that the strong-line results yielded consistently lower gas-phase C/H ratios. This suggests that the oscillator strengths may be poorly known for the weak lines. There are many archival observations of the strong lines, particularly from the *International Ultraviolet Explorer* (*IUE*), which will allow us to investigate the gas-phase carbon abundance over many new lines of sight.

In the present study, we extend the strong-line method of Sofia et al. (2011) to 15 Galactic sight lines where hydrogen is predominantly neutral and combine our results with those of Sofia et al. (2011). In order to probe the role of carbon in interstellar extinction, we have studied the variation of strength of UV extinction features with respect to the amount of carbon in the dust. Details of the observations and analysis method are given in Section 2. In Section 3, we have presented the results and discussion. In Section 4, we have summarized our conclusions.

2. OBSERVATIONS AND DATA REDUCTION

We have used archival high-resolution (R = 114,000) data from the Space Telescope Imaging Spectrograph (STIS) to determine abundances from the 1334 Å transition of C II toward 15 Galactic sight lines where interstellar C II had not been previously measured. Our target stars have all been observed with the *Far-Ultraviolet Spectroscopic Explorer* (*FUSE*) and

[4] Current address: Department of Physics, Centre for Post-Graduate Studies, Jain University, Bangalore, India.
[5] Current address: Department of Physics, Sultan Qaboos University, Muscat, Oman.

Table 1
Absorption Lines of Carbon

Transition	Vacuum Wavelength (Å)	log $f\lambda$[a]
^{12}C II	1036.3367	2.088
^{13}C II	1334.5190	2.234
^{12}C II	1334.5323	2.234
^{13}C II*	1335.6490	1.234
^{12}C II*	1335.6627	1.234
^{13}C II*	1335.6920	2.188
^{12}C II*	1335.7077	2.188
^{12}C II	2325.4029	−3.954

Note. [a] From Morton (2003).

had their total neutral hydrogen (H I + $2H_2$) column densities measured by Cartledge et al. (2004, 2006).

The data for this study are taken from the Space Telescope Science Institute (STScI) archive[6] and relied on the standard STIS pipeline calibration (Hodge et al. 1998). The spectra are all STIS echelle observations taken for one of the two *Hubble Space Telescope* (*HST*) Guest Observer programs, GO8273 or GO9855, or the *HST* SNAPSHOT program SNAP8241. The spectra were obtained through one of the two STIS setups: the $0\farcs2\times0\farcs09$ aperture with the E140H grating centered at 1271 Å or the same grating exposed through the $0\farcs2\times0\farcs2$ aperture. Details of the STIS data sets used in this study are given in Table 2. When more than one observations were made for an object, the individual spectra are merged with a weighted co-addition and the errors associated with the flux values are propagated accordingly (Bevington 1969).

We have separated the Lorentzian damping wings of the strong transition of C II from the continuum and normalized the line flux for all of the 15 sight lines. In order to fit the stellar continuum, we have used UVBLUE (Rodriguez-Merino et al. 2005),[7] a high-resolution library of synthetic spectra of stars covering the UV wavelength range. The models cover a large range of surface temperatures (T) for various surface gravities (g) and metallicities. We have further adjusted the UVBLUE spectra to account for the differences in metallicities (τ_{corr}), radial velocities of the stars (V_{rad}), and stellar rotational velocities (V_{rot}). Finally, we have normalized the model with a third-order polynomial to account for the differential reddening in the sight line and any other large-scale structure in the continuum. In order to find the best fits, we have relied on the MPFIT fitting programs of Markwardt (2009).[8] This set of IDL programs allows simultaneous optimization of multiple fit parameters (seven in our case) for a user-supplied function. The seven parameters which are simultaneously fitted during the continuum fitting procedure are τ_{corr}, V_{rad}, V_{rot}, and the four coefficients of the third-order polynomial. We have successively compared the UVBLUE models with the stellar continuum and calculated the chi-square of the best fit for each model. The model fit with the lowest chi-squared value is chosen to represent the stellar continuum and is used for normalizing the line flux. A detailed description of this procedure is given by Sofia et al. (2011). We have shown the UVBLUE model fits to the continua of the 15 lines of sight in Figure 1 and given details of the continuum fits in Table 2. We have also shown the normalized spectra in Figure 2.

In order to determine the carbon abundances along the sight lines, we have performed component profile fitting of the strong C II absorption lines. The strength of the 1334 Å transition makes it difficult to identify the absorption component structure along the line of sight and hence we have fitted the weak Mg II transitions at λλ 1239, 1240 to obtain the sight-line component structure information. We have taken the atomic constants for the carbon and magnesium transitions from Morton (2003).

We have again made use of the MPFIT routines to fit both the Mg II transitions together and optimize the fit parameters: column densities of the species, Doppler broadening parameters (b), and heliocentric velocities for multiple absorbing clouds along the line of sight. We have fitted the Mg II absorption lines with the minimum number of clouds that gave us a reasonable fit to the data. Finally, we have fitted all six carbon transitions (Table 1) together to obtain the C II and C II* column densities using the cloud structure determined from Mg II fits. For some of the sight lines, we have found it necessary to add weak components in the wings of the C II transition in order to

[6] http://archive.stsci.edu/
[7] http://www.inaoep.mx/~modelos/uvblue/uvblue.html
[8] http://purl.com/net/mpfit

Table 2
Details of Continuum Fit

Target Star	Data Set	Model Parameters T (K)	Model Parameters log g	Spectral Type[a]	Best-fit Parameters τ_{corr}	Best-fit Parameters V_{rot}	Best-fit Parameters V_{rad}	Reduced χ^2
HD 37903	O59S04010	22000	3.5	B1.5V	0.65	109	29	0.70
HD 91824	O5C095010	50000	5.0	O7V	0.38	13	−11	1.87
HD 116852	O5C01C010	16000	3.0	O9III	0.10	20	−15	0.28
HD 122879	O5C037010	17000	3.0	B0I	0.22	33	16	1.87
HD 156110	O5C01K010	20000	5.0	B3V	0.98	67	−42	1.39
HD 157857	O5C04D010	50000	5.0	O6.5III	1.02	122	69	0.84
HD 185418	O5C01Q010	29000	5.0	B0.5V	1.03	137	17	1.21
HD 192639	O5C08T010	35000	4.0	O7I	0.47	48	11	0.70
HD 198781	O5C049010	30000	4.5	B0.5V	3.42	215	−52	0.99
HD 201345	O5C050010	40000	5.0	O9V	0.42	19	44	1.88
HD 203532	O5C01S010	16000	3.5	B3IV	0.70	32	3	1.82
HD 206773	O5C04T010	31000	5.0	B0V	0.10	32	−43	0.86
HD 208440	O5C06M010	19000	3.5	B1V	0.16	25	30	1.18
HD 210809	O5C01V010	20000	5.0	O9I	0.10	25	−56	0.85
HD 232522	O5C08J010	30000	5.0	B1II	2.24	99	−29	1.07

Note. [a] From SIMBAD database.

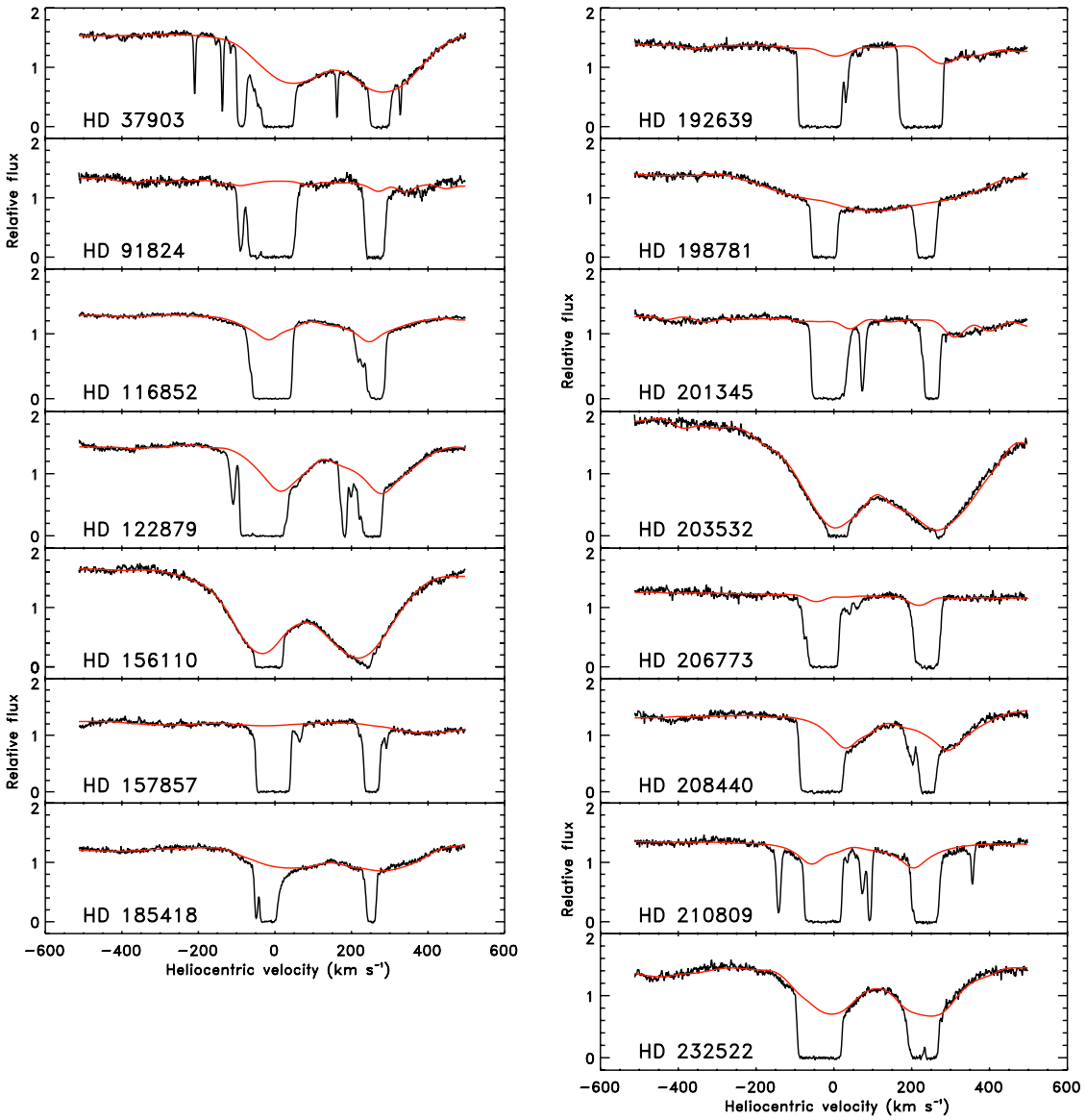

Figure 1. Continuum fits using UVBLUE models (red color) for the observational data (black color) of the 15 sight lines.
(A color version of this figure is available in the online journal.)

account for additional absorption features that are absent in the weaker magnesium transitions. These components do not add significantly to the C II abundance, but are necessary to properly fit the absorption profiles. A detailed description of the fitting procedure can also be found in Sofia et al. (2011).

We have followed the method of Sofia et al. (2011) for determining the errors associated with the carbon abundance determinations. As cautioned in that paper, it is very difficult to determine a rigorous 1σ error that accounts for the systematic errors in the determinations. Therefore, the true uncertainties may be larger than those reported here. This is particularly true for sight lines where the absorbing clouds are spread across a broad range of velocities or in sight lines where weak absorbing clouds reside in the damping wings of the dominant absorption component.

3. RESULTS AND DISCUSSION

We have listed the C II and C II* column densities along the 15 sight lines from this study as well as the six sight lines studied in Sofia et al. (2011) in Table 3. In order to make sure that we took care of all important sources of gaseous carbon, the total column densities of carbon along all of the 21 sight lines are calculated by adding contributions from C II, C II* (this study), C I (E. B. Jenkins 2009, private communication), and CO (Burgh et al. 2007; Liszt 2008; Sheffer et al. 2008). In practice, the dominant species along the line of sight were C II and C II*. As we do not expect any significant contribution to C II from the warm ionized regions (regions containing H II) along the lines of sight (Sembach et al. 2000), the C II and C II* column densities we have obtained will be from neutral H regions.

The 21 sight lines listed in Table 3 probe a variety of Galactic disk environments and include paths that range over nearly three orders of magnitude in average hydrogen density along the sight line ($\langle n(\mathrm{H})\rangle = N(\mathrm{H})/d$). For a given set of sight lines, $\langle n(\mathrm{H})\rangle$ shows the strongest correlation with the gas-phase elemental abundances (e.g., O I, Mg II, Mn II, Ni II, and P II), with Cartledge et al. (2004, 2006) determining a functional relation between the two quantities. Hence, the depletion along a given sight line can be well represented as a function of $\langle n(\mathrm{H})\rangle$. We have shown the

Table 3
Column Densities of Carbon

Target	Galactic Coordinates[a]		$\log_{10}[N(\mathrm{H})]$[b]	$\log_{10}\langle n(\mathrm{H})\rangle$[c]	$N(\mathrm{C\,II})$	$N(\mathrm{C\,II}^*)$	$N(\mathrm{C\,I})$[d]	$N(\mathrm{CO})$	Reference	$(\mathrm{C/H})_{\mathrm{gas}}$[e]	$(\mathrm{C/H})_{\mathrm{dust}}$[f]
Star	l	b	($\mathrm{cm^{-2}}$)	($\mathrm{cm^{-3}}$)	(10^{17} $\mathrm{cm^{-2}}$)	(10^{16} $\mathrm{cm^{-2}}$)	(10^{14} $\mathrm{cm^{-2}}$)	(10^{14} $\mathrm{cm^{-2}}$)		(10^{-6})	(10^{-6})
HD 37903	206.85	−16.53	21.46(0.06)	0.41	10.5(0.06)	5.04	1.75(0.13)	0.49	3	382 ± 56	82 ± 80
HD 91824	285.69	+00.06	21.16(0.05)	−0.73	2.10(0.06)	8.10	2.92(0.05)	<0.40	1	202 ± 24	262 ± 62
HD 116852	304.88	−16.13	21.02(0.08)	−1.15	1.20(1.05)	0.12	1.44(0.04)	0.20	3	116 ± 102	348 ± 117
HD 122879	312.26	+01.79	21.34(0.10)	−0.47	7.96(0.20)	0.20	2.52(0.05)	0.13	3	365 ± 94	99 ± 110
HD 156110	070.99	+35.71	20.66(0.13)	−0.69	1.25(0.05)	0.03	0.79(0.04)	...	...	275 ± 96	189 ± 112
HD 157857	012.97	+13.31	21.44(0.07)	−0.41	3.01(0.05)	0.50	4.14(0.05)	1.20	3	112 ± 19	352 ± 60
HD 185418	053.60	−02.17	21.41(0.07)	0.08	4.41(0.44)	0.28	5.34(0.06)	6.61	1	173 ± 34	291 ± 67
HD 192639	074.90	+01.47	21.48(0.07)	−0.27	3.87(0.18)	2.78	5.56(0.07)	0.60	3	138 ± 24	326 ± 62
HD 198781	099.94	+12.61	21.15(0.06)	−0.13	2.01(0.18)	6.97	3.72(0.05)	17.0	3	193 ± 31	271 ± 65
HD 201345	078.43	−09.54	21.00(0.08)	−0.90	2.89(0.02)	0.10	0.93(0.04)	<0.03	2	290 ± 58	174 ± 82
HD 203532	309.45	−31.73	21.44(0.07)	0.55	2.27(0.67)	0.12	6.38(0.10)	45.7	3	85 ± 28	379 ± 64
HD 206773	099.80	+03.61	21.25(0.05)	−0.03	7.41(0.18)	8.38	4.97(0.07)	1.58	2	464 ± 57	0 ± 81
HD 208440	104.02	+06.43	21.32(0.08)	0.04	2.70(0.16)	0.12	6.87(0.10)	1.58	2	131 ± 27	333 ± 63
HD 210809	099.84	−03.12	21.33(0.08)	−0.70	6.61(0.59)	2.42	5.07(0.20)	0.23	3	321 ± 70	143 ± 90
HD 232522	130.69	−06.71	21.19(0.05)	−0.92	4.81(0.39)	0.88	3.96(0.12)	...	...	317 ± 46	147 ± 73
HD 27778[g]	172.76	−17.39	21.36(0.08)	0.53	1.99(0.60)	0.02	11.4(0.10)	120	2	93 ± 32	371 ± 65
HD 37021[g]	209.00	−19.38	21.68(0.12)	0.61	4.35(1.20)	0.29	0.44(0.05)	...	...	92 ± 38	372 ± 69
HD 37061[g]	208.92	−19.27	21.73(0.09)	0.66	5.27(1.50)	0.41	0.94(0.04)	...	...	99 ± 36	365 ± 67
HD 147888[g]	353.64	+17.70	21.77(0.08)	1.11	5.66(0.80)	0.39	4.96(0.05)	19.1	3	98 ± 23	366 ± 62
HD 152590[g]	344.84	+01.82	21.47(0.05)	−0.28	6.29(1.40)	0.37	4.05(0.08)	0.59	3	215 ± 54	249 ± 79
HD 207198[g]	103.13	+06.99	21.68(0.09)	0.40	3.23(0.70)	0.16	17.7(0.10)	31.6	2	69 ± 21	395 ± 61

Notes.
[a] From SIMBAD database.
[b] $\log_{10}[N(\mathrm{H})]$ values are obtained from Cartledge et al. (2004, 2006).
[c] $\log_{10}\langle n(\mathrm{H})\rangle$ values are obtained from Cartledge et al. (2004, 2006).
[d] $N(\mathrm{C\,I})$ values are obtained from E. B. Jenkins (private communication).
[e] The total C in gas includes carbon contained by C II, C II*, C I, and CO.
[f] Dust-phase abundance determination of carbon is based on a reference abundance of 464 ppm and would be reduced by 176 if the solar abundance of carbon reported by Lodders (2003) was used as the reference abundance.
[g] C II and C II* column densities are taken from Sofia et al. (2011).
References. (1) Burgh et al. 2007; (2) Liszt 2008; (3) Sheffer et al. 2008.

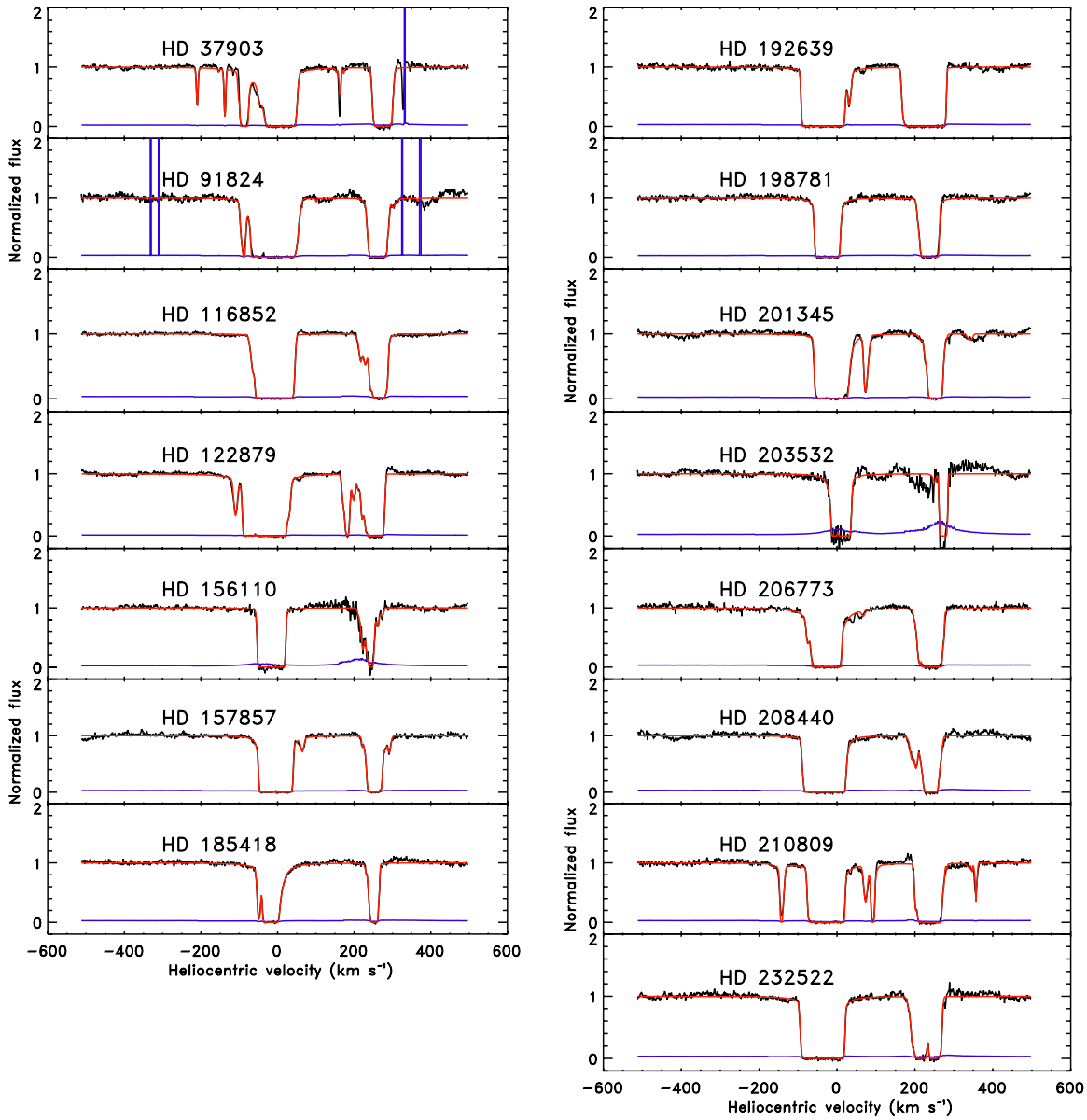

Figure 2. Normalized 1334 Å C II transitions along the 15 lines of sight (black) and multi component fits to the transitions (red). Lines shown in blue represent normalized errors corresponding to the normalized flux values.

number of carbon atoms in the gas-phase per million hydrogen atoms (ppm) plotted as a function of log $\langle n(\mathrm{H})\rangle$ in Figure 3. Except for the points corresponding to HD 37903, HD 116852, and HD 206773, the gas-phase C/H ratio shows a decreasing trend for increasing values of log $\langle n(\mathrm{H})\rangle$. Similar variations have been observed for O I, Mg II, and other depleted species (Cartledge et al. 2004, 2006).

The total abundance of carbon in the ISM is a sum of the components residing in the gas and in the dust. Therefore, in order to calculate the dust-phase abundances of carbon from the gas-phase abundances, we need a reference carbon abundance to substitute for the total carbon abundance in the ISM. Traditional reference abundances used in the ISM studies are the elemental abundances in the proto-Sun (Lodders 2003) and young F and G star abundances (Sofia & Meyer 2001), but it is evident from Figure 3 that several of the sight lines have gas-phase carbon abundances higher than these. However, all of these targets, except HD 37903 and HD 206773, also have 1σ error bars that will bring them within the solar carbon abundance. Interestingly, the sight line toward HD 206773 is found to be significantly reddened ($E(B-V) = 0.45$) despite its large gas-phase carbon abundance. We note that the 1334 Å feature toward this star has weak components in both the short- and long-wavelength damping wings of the absorption. As mentioned above, absorption superimposed on the main damping wings increases the systematic errors (not included in the error bars), which likely accounts for the high measured abundance here. HD 37903 has its C II absorption spread over a wide range of heliocentric velocities, which will make the systematic uncertainties large in the carbon abundance determination in this sight line. Finally, we note that the systematic uncertainties are also likely high toward HD 210809, where the absorption is spread over a wide velocity range.

For our discussion below, we have assumed that the high value of gas-phase C/H ratio toward HD 206773 (C/H = 464 ± 57 ppm) represents the lower limit for the interstellar cosmic carbon abundance. We did this for convenience as this value allows for dust abundances to be calculated for our data set

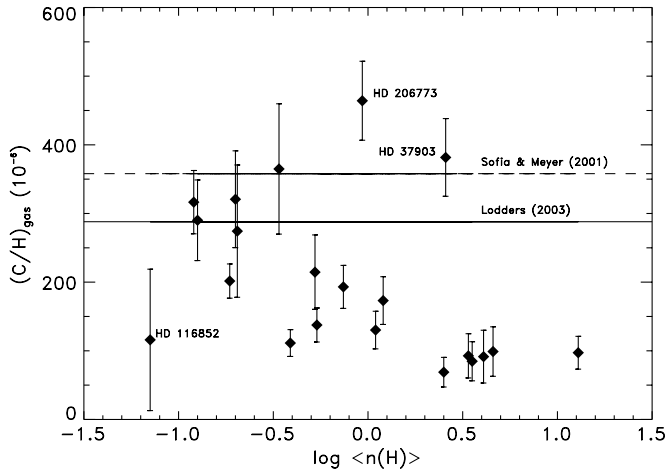

Figure 3. Gas-phase C/H ratio plotted as a function of the logarithm of average density of hydrogen along the line of sight. Associated uncertainties in $(C/H)_{gas}$ are also shown in the figure. The solid line at 288 ppm in the figure represents solar system abundance of carbon (Lodders 2003) and the solid dashed line at 358 ppm represents the young F and G star abundance of carbon (Sofia & Meyer 2001).

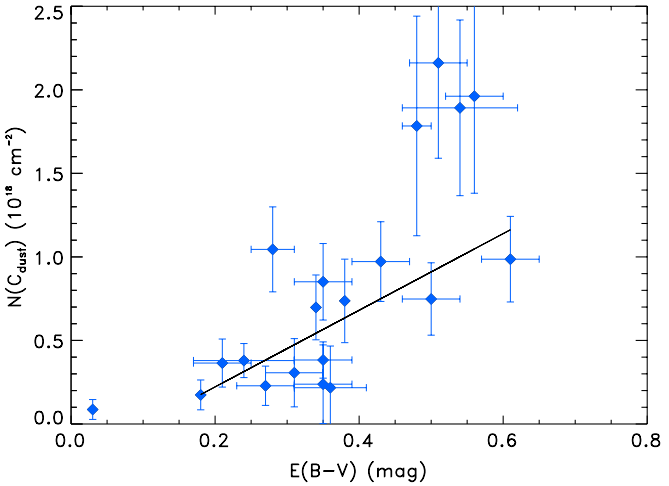

Figure 4. $N(C_{dust})$ plotted as a function of $E(B-V)$. Associated uncertainties in $E(B-V)$ and $N(C_{dust})$ are also shown in the figure. A correlation is found between $N(C_{dust})$ and $E(B-V)$ with a value of 0.71 for the correlation coefficient. The linear least-squares fit to the points excluding the one at bottom left is also shown in the figure.

(A color version of this figure is available in the online journal.)

with none having negative values. The choice of this reference abundance versus another, such as solar, does not change our general results. We have calculated the dust-phase abundance of carbon along all the 21 sight lines and then calculated the column density of carbon in dust ($N(C_{dust})$) therein. We have plotted $N(C_{dust})$ against $E(B-V)$ in Figure 4. There is a general trend in increased carbon atoms in dust as a function of $E(B-V)$. Although there is no reason to expect a linear correlation, we have performed a linear fit over the points, excluding the one in the bottom left in order to show this relationship. With values of 1.7 and 0.71 for the reduced chi-square and the linear correlation coefficient, respectively, our data show that carbon is related to extinction. Given the number of data points and the error bars, there is no justification in fitting a higher order polynomial to the data. The increase in the incorporation of carbon into dust with increased $E(B-V)$ agrees with Jenkins (2009), who finds that all of the depleted elements follow a pattern together of increasing or decreasing dust incorporation.

We have repeated the correlation studies by choosing Lodders (2003) protosolar abundance as a reference, in order to check the robustness of our results. Though the points in Figure 4 would move down with this reference abundance (the upper points moving down more than the lower points), there is still the increasing trend in C dust abundance with $E(B-V)$, which can be fit with a linear correlation coefficient that does not change greatly from that determined with the HD 206773 reference abundance.

Other important elements in dust are O, Mg, Fe, and Si. Although the depletion fractions of C and O are often less than those of Mg, Fe, and Si, their large abundances in the ISM likely makes them the most abundant elements in interstellar dust. The ISM reference abundance of oxygen is still uncertain. When the solar abundances are chosen, the calculated depletion of oxygen is twice as large as the abundance of oxygen obtained from all available sources of oxygen containing dust (Jenkins 2009). Given the large uncertainty in the O abundance in dust, the large values of dust-phase column densities of carbon shown in Table 3 suggest that carbon could be the most abundant element in interstellar dust.

Fitzpatrick & Massa (1988, hereafter referred to as FM88) found an empirical fit for extinction curves,

$$\frac{E(\lambda-V)}{E(B-V)} = c_1 + c_2\lambda^{-1} + c_3 D(\lambda^{-1}, \gamma, \lambda_0^{-1}) + c_4 F(\lambda^{-1}). \quad (1)$$

Here, c_1 and c_2 define the linear background; c_3 and c_4 define the strengths of the 2175 Å bump and the FUV curvature, respectively; $D(\lambda^{-1}, \gamma, \lambda_0^{-1})$ defines the shape of the bump with γ and λ_0^{-1} representing the FWHM and center of the bump, respectively; and $F(\lambda^{-1})$ defines the FUV curvature. In order to probe the role of carbon in interstellar UV extinction, we have studied the variation of the strength of the FM88 UV extinction features with respect to the amount of carbon in the dust. We note that a change in the reference abundance will move the points up or down in Figures 5–7 by equal amounts, i.e, the relative locations of the points with respect to each other will not change. A list of extinction parameters (Valencic et al. 2004) used in this study is given in Table 4 for all the target stars.

The grain-size distribution along a line of sight is characterized by $R_V = A_V/E(B-V)$. Small grains preferentially absorb UV to visible light and make a relative increase in the UV to visual extinction. As the grains grow bigger in size, they produce considerable extinction to the visible light also. As a result, the difference between extinctions in the UV and visible wavelengths becomes small. We have plotted $(C/H)_{dust}$ as a function of R_V^{-1} in Figure 5. c_4/R_V represents the FUV extinction parameter of the extinction curve normalized to A_V, whereas the FUV extinction parameter of the extinction curve normalized to $E(B-V)$ is represented by c_4. Instead of FM88 c_3 and c_4, we have used c_3/R_V and c_4/R_V in this work because $E(B-V)$ is relative while A_V is absolute. A representation of $(C/H)_{dust}$ plotted as a function of c_4/R_V is shown in Figure 6. Not surprisingly, the variation observed for c_4/R_V is similar to the variation of R_V^{-1}. This agrees with the reported correlation between c_4 and R_V^{-1} by Cardelli et al. (1988, 1989) and Jenniskens & Greenberg (1993) as well as with the finding of a correlation by Valencic et al. (2004) between c_4/R_V and R_V^{-1}. Variation of the 2175 Å bump strength normalized to A_V (c_3/R_V), as shown in Figure 7,

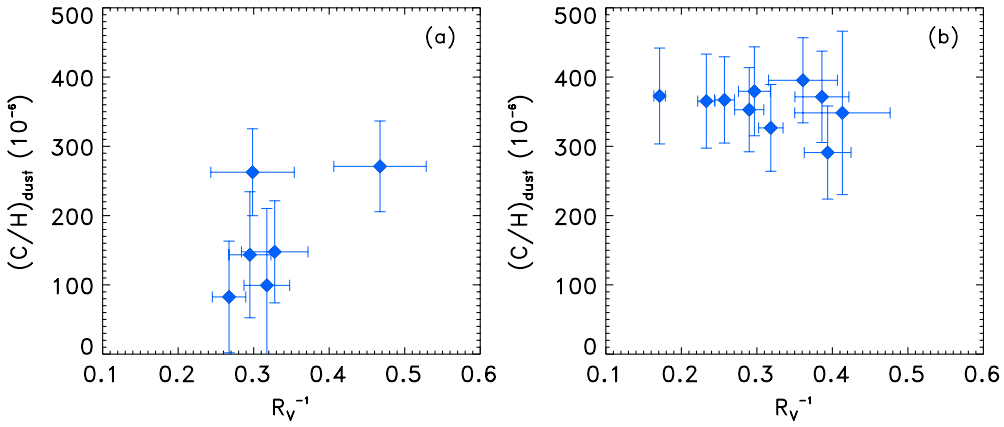

Figure 5. $(C/H)_{dust}$ plotted as a function of R_V^{-1}. Associated uncertainties in R_V^{-1} and $(C/H)_{dust}$ are also shown in the figure. For the sake of clarity, the lower density (a) and denser (b) regions are shown separately. For further explanation, please see the text.

(A color version of this figure is available in the online journal.)

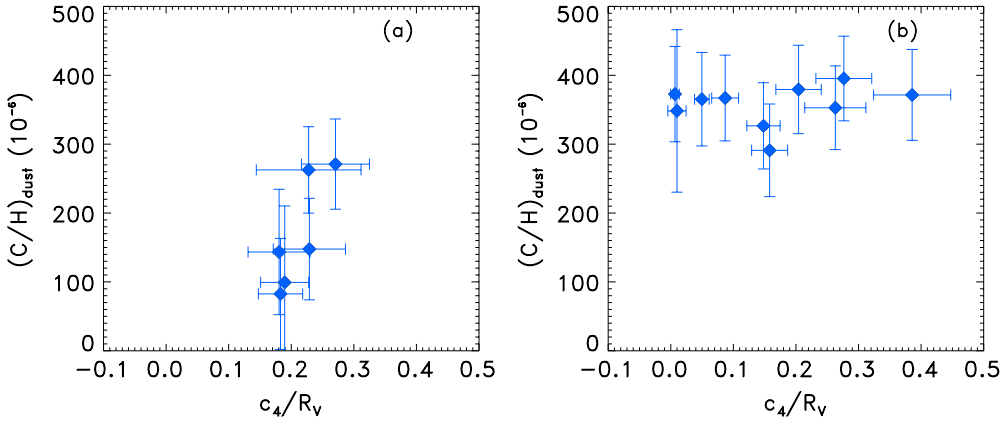

Figure 6. $(C/H)_{dust}$ plotted as a function of c_4/R_V. Associated uncertainties in c_4/R_V and $(C/H)_{dust}$ are also shown in the figure. Like in Figure 5, the lower density (a) and denser (b) regions are shown separately.

(A color version of this figure is available in the online journal.)

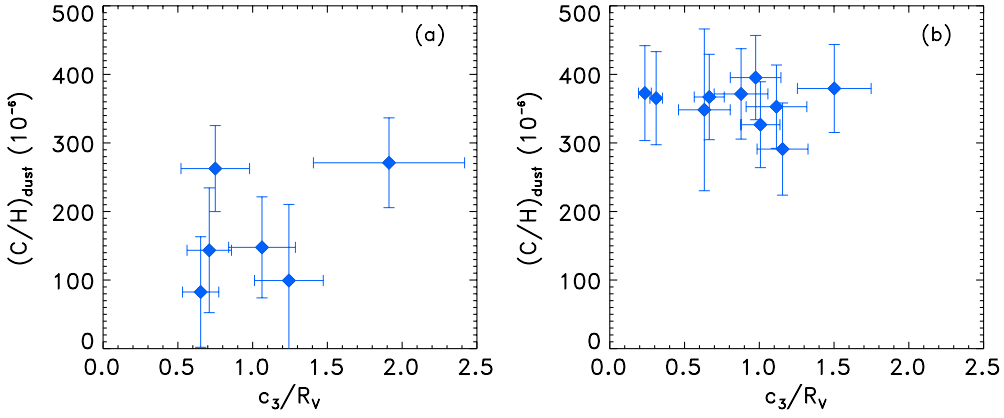

Figure 7. $(C/H)_{dust}$ plotted as a function of c_3/R_V. Associated uncertainties in c_3/R_V and $(C/H)_{dust}$ are also shown in the figure. Once again, the lower density (a) and denser (b) regions are shown separately.

(A color version of this figure is available in the online journal.)

bears some resemblance to the variations of R_V^{-1} and c_4/R_V with the abundance of carbon in dust. We have shown separately the lower density and higher density sight lines as indicated by C incorporated into dust, in all three figures (Figures 5–7), in order to make the trend more evident for the readers. The line of separation between lower and higher density regions is fixed at 290 ppm in accordance with the simultaneous optimization of linear correlation coefficients of the points that will eventually go into Figures 5(a), 6(a), and 7(a).

From Figure 5, it can be seen that R_V^{-1} shows an increasing trend with $(C/H)_{dust}$ until about 290 ppm and after that the plot is a scatter. The observed variation in R_V^{-1} with $(C/H)_{dust}$ indicates that in higher density environments (where we have a larger fraction of the C in dust) both big and small grain populations

Table 4
Sight Line and Extinction Curve Properties

Target Star	Distance (d) (kpc)	$E(B-V)$ (mag)	A_V (mag)	R_V	c_3/R_V	c_4/R_V	Gamma (γ)
HD 37903	0.74	0.35(0.04)	1.31	3.74(0.31)	0.6524(0.1213)	0.1828(0.0354)	0.9230(0.0280)
HD 91824	3.53	0.24(0.07)	0.80	3.35(0.62)	0.7501(0.2292)	0.2278(0.0837)	0.8710(0.0290)
HD 116852	4.83	0.21(0.04)	0.51	2.42(0.37)	0.6326(0.1730)	0.0099(0.0146)	0.7820(0.0690)
HD 122879	2.26	0.36(0.05)	1.13	3.15(0.30)	1.2425(0.2297)	0.1895(0.0385)	0.8310(0.0210)
HD 156110[a]	0.72[b]	0.03[b]	...	...	...	...	...
HD 157857	1.90	0.43(0.04)	1.48	3.45(0.23)	1.1148(0.2031)	0.2629(0.0488)	0.8480(0.0280)
HD 185418	0.91	0.50(0.04)	1.27	2.54(0.20)	1.1555(0.1704)	0.1579(0.0288)	0.8190(0.0240)
HD 192639	1.00	0.61(0.04)	1.91	3.14(0.16)	1.0076(0.1303)	0.1481(0.0266)	0.8660(0.0290)
HD 198781	0.73	0.35(0.04)	0.75	2.14(0.28)	1.9121(0.5055)	0.2706(0.0543)	1.1250(0.0670)
HD 201345[a]	2.57[b]	0.18[b]	0.51[c]	...	...	...	...
HD 203532	0.21	0.28(0.03)	0.94	3.37(0.24)	1.5015(0.2464)	0.2042(0.0363)	1.2660(0.0400)
HD 206773	0.60	0.45(0.04)	1.99	4.42(0.26)	0.5041(0.0784)	0.0486(0.0150)	0.8930(0.0300)
HD 208440[a]	0.62[b]	0.34[b]	...	...	...	...	...
HD 210809	3.96	0.31(0.04)	1.05	3.39(0.32)	0.7100(0.1487)	0.1805(0.0496)	0.8440(0.0300)
HD 232522	5.44	0.27(0.04)	0.82	3.05(0.41)	1.0626(0.2234)	0.2289(0.0577)	0.9340(0.0310)
HD 27778	0.33	0.35(0.04)	0.91	2.59(0.24)	0.8780(0.1797)	0.3857(0.0616)	0.9740(0.0320)
HD 37021	0.68	0.48(0.02)	2.80	5.84(0.26)	0.2349(0.0427)	0.0067(0.0070)	1.0810(0.0360)
HD 37061	0.34	0.56(0.04)	2.40	4.29(0.21)	0.3103(0.0418)	0.0497(0.0117)	0.9010(0.0290)
HD 147888	0.18	0.51(0.04)	1.99	3.89(0.20)	0.6653(0.1004)	0.0869(0.0215)	0.8790(0.0290)
HD 152590[a]	1.80[b]	0.38[b]	...	...	...	...	...
HD 207198	1.21	0.54(0.08)	1.50	2.77(0.35)	0.9755(0.1692)	0.2765(0.0446)	0.8830(0.0240)

Notes.
[a] Except for these sight lines, the tabulated values are all obtained from Valencic et al. (2004).
[b] Distance and $E(B-V)$ of the sight lines are obtained from Cartledge et al. (2004).
[c] A_V is obtained from Schröder et al. (2004).

exist. Cardelli et al. (1988) and Mathis & Whiffen (1989) have independently calculated the linear UV background extinction using FM88 fit and found a decrease in linear UV extinction in dense media. Our present findings are consistent with the Cardelli et al. (1988) and Mathis & Whiffen (1989) results and we propose that the bigger grains formed in dense molecular clouds get disrupted to smaller grains as they circulate to the less dense layers of the cloud. As the nonlinear FUV extinction is a consequence of the presence of small grains in the ISM, a gradual decrease in FUV extinction with decrease in density (Figure 6) indicates the preferential disruption of smaller grains into gas in the diffuse ISM.

Figure 7 shows no detectable correlation between the c_3/R_V parameter and the abundance of carbon in dust. This is surprising given that the dust models of Draine & Li (2007) attribute the 2175 Å bump to the π–π^* excitations in aromatic carbon. Further studies by Cecchi-Pestellini et al. (2008) have suggested that mixtures of polycyclic aromatic hydrocarbons (PAHs) can accurately account for the UV bump and the nonlinear FUV rise in the extinction curve, and the PAH charge state is linked to the relative intensity of the two features. If PAHs are responsible for the bump, then one might also expect a correlation between the size of the grain population and the strength of the bump. Valencic et al. (2004) do find a weak correlation between the FM88 c_3/R_V (bump) and c_4/R_V (FUV strength) parameters, but our data are not sufficient in number or quality to make such a determination.

4. SUMMARY

In this paper, we have presented the abundances of carbon in both gas and dust phases of the ISM along 21 Galactic sight lines, 15 of which are first-time measurements. Our results confirm that carbon can be a dominant constituent of interstellar dust. Our correlation studies indicate the presence of both big and small grain populations in environments with large $(C/H)_{dust}$. This agrees with the suggestions of previous authors that big grains form in dense clouds and then fragment into smaller grains as they reach the lower density regions along the line of sight. We suggest that the reason for a gradual decrease in the FUV extinction parameter in lower density environments could be the preferential disruption of smaller grains into gas as they reach the diffuse ISM. We have found no correlation between the strength of the 2175 Å bump and the abundance of carbon in dust or the size distribution of grains. This result is surprising given that many models now invoke PAHs as the bump carrier and we look forward to further observations and analysis to confirm this.

We are thankful to E. B. Jenkins for sending us the results of his C I column density measurements and to the anonymous referee for his valuable comments and suggestions. This work is supported by the funds received from cycle 17 Hubble Space Telescope program (HST-AR-11775) and from the Council of Scientific and Industrial Research (CSIR), India. V.S.P. is grateful to Indian Institute of Astrophysics for hospitality during this work.

Facilities: HST (STIS)

REFERENCES

Bakes, E. L. O., & Tielens, A. G. G. M. 1994, ApJ, 427, 822
Bevington, P. R. 1969, Data Reduction and Error Analysis for the Physical Sciences (New York: McGraw-Hill)
Burgh, E. B., France, K., & McCandliss, S. R. 2007, ApJ, 658, 446
Cardelli, J. A., Clayton, G. C., & Mathis, J. S. 1988, ApJ, 329, L33
Cardelli, J. A., Clayton, G. C., & Mathis, J. S. 1989, ApJ, 345, 245
Cardelli, J. A., Mathis, J. S., Ebbets, D. C., & Savage, B. D. 1993, ApJ, 402, L17

Cardelli, J. A., Meyer, D. M., Jura, M., & Savage, B. D. 1996, ApJ, 467, 334
Cartledge, S. I. B., Lauroesch, J. T., Meyer, D. M., & Sofia, U. J. 2004, ApJ, 613, 1037
Cartledge, S. I. B., Lauroesch, J. T., Meyer, D. M., & Sofia, U. J. 2006, ApJ, 641, 327
Cecchi-Pestellini, C., Malloci, G., Mulas, G., Joblin, C., & Williams, D. A. 2008, A&A, 486, L25
Draine, B. 1989, in IAU Symp. 135, Interstellar Dust, ed. L. J. Allamandola & A. G. G. M. Tielens (Dordrecht: Kluwer), 313
Draine, B. T., & Li, A. 2007, ApJ, 657, 810
Duley, W. W., & Williams, D. A. 1981, MNRAS, 196, 269
Dwek, E., Arendt, R. G., Fixsen, D. J., et al. 1997, ApJ, 475, 565
Fitzpatrick, E. L., & Massa, D. 1988, ApJ, 328, 734
Hobbs, L. M., York, D. G., & Oegerle, W. 1982, ApJ, 252, L21
Hodge, P., Baum, S., McGrath, M., et al. 1998, Instrument Science Report STIS 98-10 (Baltimore: Space Telescope Science Institute), 15
Jenkins, E. B. 2009, ApJ, 700, 1299
Jenniskens, P., & Greenberg, J. M. 1993, A&A, 274, 439
Joblin, C., Leger, A., & Martin, P. 1992, ApJ, 393, L79
Liszt, H. S. 2008, A&A, 492, L743
Lodders, K. 2003, ApJ, 591, L1220
Markwardt, C. B. 2009, in ASP Conf. Ser. 411, Astronomical Data Analysis Software and Systems, ed. D. A. Bohlender, D. Durand, & P. Dowler (San Francisco, CA: ASP), 251
Mathis, J. S., & Whiffen, G. 1989, ApJ, 341, 808
Morton, D. C. 2003, ApJ, 149S, 205
Rodriguez-Merino, L. H., Chavez, M., Bertone, E., & Buzzoni, A. 2005, ApJ, 626, 411
Schröder, S. E., Kaper, L., Lamers, H. J. G. L. M., & Brown, A. G. A. 2004, A&A, 428, 149
Sembach, K. R., Howk, J. C., Ryans, R. S. I., & Keenan, F. P. 2000, ApJ, 528, 310
Sheffer, Y., Rogers, M., Federman, S. R., et al. 2008, ApJ, 687, 1075
Snow, T. P., & Bierbaum, V. M. 2008, Annu. Rev. Anal. Chem., 1, 229
Sofia, U. J., Cardelli, J. A., Guerin, K. P., & Meyer, D. M. 1997, ApJ, 482, L105
Sofia, U. J., Fitzpatrick, E., & Meyer, D. M. 1998, ApJ, 504, L47
Sofia, U. J., Lauroesch, J. T., Meyer, D. M., & Cartledge, S. I. B. 2004, ApJ, 605, 272
Sofia, U. J., & Meyer, D. M. 2001, ApJ, 554, L221
Sofia, U. J., Parvathi, V. S., Babu, B. R. S., & Murthy, J. 2011, AJ, 141, 22
Valencic, L. A., Clayton, G. C., & Gordon, K. D. 2004, ApJ, 616, 912